applied sciences

MDPI

Article

Wear Characteristics of (Al/B_4C and Al/TiC) Nanocomposites Synthesized via Powder Metallurgy Method

Lamyaa Khaleel Hasan [1], Suaad Makki Jiiad [1], Khansaa Dawood Salman [2], Wisam Abed Kattea Al-Maliki [3,4], Falah Alobaid [4,*] and Bernd Epple [4]

1 Department of Electromechanical Engineering, University of Technology-Iraq, Ministry of Higher Education & Scientific Research, Baghdad 10066, Iraq
2 Department of Aeronautical Techniques Engineering, Bilad Alrafidain University College, Diyala 32001, Iraq
3 Mechanical Engineering Department, University of Technology-Iraq, Ministry of Higher Education & Scientific Research, Baghdad 10066, Iraq
4 Institut Energiesysteme und Energietechnik, Technische Universität Darmstadt, Otto-Berndt-Straße 2, 64287 Darmstadt, Germany
* Correspondence: falah.alobaid@est.tu-darmstadt.de; Tel.: +49-6151-16-6691; Fax: +49-6151-16-5685

Abstract: Objective: The aim of the present work is to study the microstructure, wear behavior, physical properties, and micro-hardness of the aluminum matrix AA6061 reinforced with TiC and B_4C nanoparticles with different concentrations of 2.5, 5, 7.5, 10, and 12.5 wt.%. Methodology: Al/B_4C and Al/TiC nanocomposites were fabricated with a powder metallurgy route. A dry sliding wear test was performed with a pin-on-disc machine. The wear test was performed at the applied loads of 3, 6, 9, 12, and 15 N at a constant time for about 10 min. The microstructural analysis of the fabricated nanocomposites was examined via field emission scanning electron microscopy (FESEM) and X-ray diffraction (XRD) analysis. The obtained data: The results of this work show that increasing the applied load leads to a decrease in the wear rate of the aluminum matrix and its nanocomposites. The wear rate of the aluminum matrix without any additives is about 7.25×10^{-7} (g/cm), while for Al/TiC and Al/B_4C, it is 5.1×10^{-7} (g/cm) and 4.21×10^{-7} (g/cm), respectively. An increment in B_4C percent increases the actual density, while an increment in TiC percent minimizes the actual density at 2.90 g/cm^3 and 2.51 g/cm^3, respectively. An increment in B_4C percent decreases by 4.61%, while the porosity slightly increases with increases in TiC percent of 6.2%. Finally, the micro-hardness for Al/B_4C is about 92 (HRC), and for Al/TiC, it is about 87.4 (HRC). Originality: In the present work, nanocomposites were fabricated using a powder metallurgy route. Fabricated nanocomposites are important in engineering industries owing to their excellent wear resistance, low thermal distortion, and light weight compared with other nanocomposites. On the other hand, Al/B_4C and Al/TiC nanocomposites fabricated with a powder metallurgy route have not previously been investigated in a comparative study. Therefore, an investigation into these nanocomposites was performed.

Keywords: nanocomposites; powder metallurgy; microstructure; physical properties; micro-hardness; wear

check for updates

Citation: Hasan, L.K.; Jiiad, S.M.; Salman, K.D.; Al-Maliki, W.A.K.; Alobaid, F.; Epple, B. Wear Characteristics of (Al/B_4C and Al/TiC) Nanocomposites Synthesized via Powder Metallurgy Method. *Appl. Sci.* **2023**, *13*, 12939. https://doi.org/10.3390/app132312939

Academic Editor: Ana Martins Amaro

Received: 2 October 2023
Revised: 26 October 2023
Accepted: 31 October 2023
Published: 4 December 2023

1. Introduction

Nanocomposite materials are defined as advanced materials containing multiphases; one of them is known as a matrix while the other is known as a reinforcement material. The reinforcement materials are nano-sized and can be incorporated as nanoparticles, nanorods, nanofibers, or nanoplatelets [1].

The matrix can be used as a metal, ceramic, or polymer with additive nano-sized materials to produce nanocomposites. Nanocomposites have been manufactured via a solid state such as a powder metallurgy route or a liquid state such as a casting route to achieve special characteristics for advanced engineering applications [2]. The manufactured nanocomposite has a new microstructure owing to the rearrangement of the constituent elements, which in turn improves the physical, thermal, electrical, mechanical, wear, and corrosion resistance. The properties of the manufactured nanocomposite are different compared with the original materials, either the properties of the matrix or the properties of the additive nano-sized materials. In recent years, great attention has been paid to the manufacturing of metal matrix nanocomposites with different types of reinforcement materials, mainly ceramic nanomaterials [3,4].

Commonly, aluminum and aluminum alloys are used as metal matrixes because of their exceptional characteristics, such as low density, low cost, high strength, and high wear resistance. These characteristics create new properties for the produced nanocomposites, which can be used in many advanced engineering applications, such as in the aerospace, automotive, and marine industries [5,6]. Currently, hybrid nanocomposites have been produced for many multifunctional applications, such as in the communication, renewable energy, optical, and medical sectors. In hybrid nanocomposites, there are many reinforcement materials that can be used at the same time to improve the desired properties. There are many parameters affecting the properties of hybrid nanocomposites, such as the size and shape of the reinforcement materials and the weight percentage of the additive materials. Also, the properties of the matrix, the created binding between the matrix and reinforcement materials, and the route used for producing the hybrid nanocomposites are directly affected by the final properties of the hybrid nanocomposites. Commonly, the hybrid nanocomposites have been produced with solid-state or liquid-state routes [7–10].

Powder technology is widely used to manufacture metal matrix composites because of its exceptional properties to fabricate engineering components with exact dimensions. In recent decades, powder technology has been greatly applied to produce metal matrix composites compared to casting techniques. The engineering parts manufactured with powder technology have excellent properties such as high strength, good wear, and corrosion resistance. With this technique, the reinforcement materials are uniformly distributed in the matrix with a small amount of porosity, improving many of the properties. Compared with the casting technique, the reinforcement materials are aggregated and create a weak binding with the matrix [11]. The aluminum AA6061 alloy is commonly used for many applications, like automobile parts, marine technology, aerospace technology, aeronautical technology, and electronics, which need special characteristics like high thermal, electrical, and mechanical properties. To enhance these properties, the Al alloy must be reinforced by many materials such as metals, polymers, and ceramics (carbides, nitrides, and oxides) to obtain aluminum nanocomposites (ANCs) [12]. Aluminum nanocomposites (ANCs) are a mixture of many component phases, in which aluminum metal is a matrix reinforced by ceramic materials such as Al_2O_3, Fe_2O_3, MgO, TiO_2, TiC, SiC, B_4C, etc. However, these additive materials improve mechanical, physical, and thermal properties [13,14]. Therefore, improving the mechanical properties of Al alloys by adding reinforcing materials such as ceramics creates many difficulties through the working or machining of the synthesized nanocomposites. Therefore, ceramic additives must be introduced at a high accuracy of concentration to improve the mechanical and thermal characteristics of ANCs. Aluminum nanocomposites have been produced with many different methods, such as liquid-phase and solid-phase methods. Liquid-phase methods include casting and stir casting, while solid-phase methods include powder metallurgy [15]. Also, these processing methods involve many imperfections, like impurities, dislocations, brittle inclusions, and porosity, which make the ceramic nanoparticles heterogeneously dispersed in an aluminum alloy. At the same time, dislocations form in ANCs, perhaps owing to the differences in the thermal properties of aluminum and the additive nanoparticles [16]. These inclusions minimize wear resistance and strength, and in turn, diminish the performance of ANCs during the service. Moreover, the low wettability on the interfacial Al matrix and ceramic nanoparticles leads to diminished interface bindings between the Al matrix and the ceramic nanoparticles, hence limiting the usage of ANCs. AA6061 is an important alloy owing to its unique properties such as high strength, high resistance to corrosion and wear, low density, and high creep resistance. Therefore, this alloy can be used in various applications at elevated temperatures when reinforced by ceramic nanoparticles. The characteristics of ANCs are widely defined by the microstructure and chemical composition of aluminum alloys. The reinforcement additive materials are distinguished by their weight percentages and dispersion, which are extremely affected by the physical and mechanical properties, the cost of nanocomposites, and their performance [17].

The powder metallurgy technique is the best processing method to synthesize ANCs due to the easy-to-manufacture nanocomposites and it is suitable for producing different nanocomposites that cannot be produced in the liquid phase. On the other hand, it is used to produce nanocomposites with precision dimensions and can be used for many different alloys. Furthermore, it has good wettability at the interfaces between reinforcing nanoparticles and the Al matrix [18]. Many investigations have been made about Al alloys reinforced with ceramic nanoparticles. Wang et al. prepared an Al/Al_2O_3 composite material by powder technology. The effect of Al_2O_3 and different sintering temperatures (550 °C and 650 °C) on the mechanical properties and wear characteristics of ANCs have been investigated. Al_2O_3 has been incorporated by weight percentage at 20 wt.%. The results of this investigation show improvements in sintered density, micro-hardness, and wear resistance at 650 °C. This leads to strong interfacial bindings between Al_2O_3 particles and the Al matrix. The images of the SEM examination show a uniform dispersion of Al_2O_3 into the Al matrix [19]. B. Venkatesh and B. Harish studied the mechanical characteristics of Al alloy reinforcing with SiCp nanoparticles manufactured by the powder technology method. The resultant data of this investigation show that SiCp particles are uniformly dispersed into the Al matrix with low porosities and enhance mechanical properties such as strength and micro-hardness [20]. A. Thangarasu et al. investigated the microstructure, wear characteristics and mechanical properties of Al/TiC composite manufacturing by friction stir processing (FSP). The obtained resultant data from this work show enhancements in wear and mechanical characteristics such as the strength and hardness of the fabricated composites [21]. Manohar et al. have studied the effect of graphite and SiC on the microstructure and mechanical characteristics of the hybrid nanocomposite. SiC was added by a constant volume percent of 2 vol.%, while graphite was incorporated by different volume percentages at 2, 4, 6, 8, and 10 vol.%. These additive reinforcing materials will improve mechanical characteristics such as micro-hardness and compressive strength. The manufactured hybrid nanocomposites were produced by powder technology under applied pressure at 430 MPa, while the sintering process was carried out in an electrical furnace at 550 °C under an argon atmosphere to prevent the oxidation of the specimens. The results of this work show that the reinforcement materials were homogeneously dispersed in the aluminum matrix, which in turn improved the mechanical characteristics [22]. Negin Ashrafi et al. manufactured the hybrid nanocomposites Al/Fe_3O_4/SiC via the powder technology method. This investigation has studied the effect of Fe_3O_4 and SiC on their physical and mechanical properties. Fe_3O_4 was incorporated by 15 wt.% and 30 wt.%, while SiC was added by a constant percent of 20 wt.%. Magnesium stearate was added as an activator material to prevent the accumulation of the reinforcement nanomaterials during the mixing process. SEM photomicrographs show that Fe_3O_4 and SiC are homogeneously distributed into the aluminum matrix. The preferred density and micro-hardness for Al/30 wt.% Fe_3O_4/20 wt.% SiC after the sintering process were 2.69 g/cm^3 and 91 HV, respectively. Moreover, the wear rate decreased from 0.601 to 0.412 and the corrosion resistance from 90.91% to 99.83%, respectively [23]. Gang Li and Bowen Xiong have produced aluminum reinforced by graphene nanosheets using powder technology. Graphene nanosheets were introduced into the aluminum matrix by 0.25 wt.%, 0.5 wt.% and 1.0 wt.%. The effect of graphene nanosheets on microstructure and mechanical properties was investigated. The results of scanning electron microscopy (SEM), X-ray diffraction (XRD), and transmission electron microscopy (TEM) examinations show a homogeneous dispersion of graphene nanosheets into the aluminum matrix. Additionally, XRD examination shows that the Al_4C_3 phase was created at the interfaces between graphene nanosheets and aluminum atoms. Also, the results show an improvement in mechanical properties such as micro-hardness, yield strength, and tensile strength with the addition of graphene nanosheets. This study emphasizes that the referred portion of graphene nanosheets is 0.25 wt.% [24]. A. Makkia et al. studied the physical properties, mechanical properties, and microstructure of aluminum nanocomposite manufactured by powder metallurgy. Nickel ferrite ($NiFe_2O_4$) nanoparticles at 35 nm have been incorporated at different percents (0 wt.%, 1 wt.%, 2.5 wt.%, 5 wt.%, and 10 wt.%). The mechanical and magnetic properties of the manufactured nanocomposites were defined. The microstructural analysis for the manufactured nanocomposites was conducted by FESEM, XRD, and DSC examinations, while the magnetic properties were defined by VSM examination. The results of this investigation show that the increasing weight percent (5 wt.%) of $NiFe_2O_4$ ceramic nanoparticles will increase yield strength, tensile strength, and micro-hardness. FESEM images show a homogeneous dispersion of $NiFe_2O_4$ ceramic nanoparticles into the aluminum matrix and then improve the density of nanocomposites for green compacts and sintered specimens. Moreover, increasing $NiFe_2O_4$ to 0 wt.% will increase the magnetization, and compressive strength and decrease the elongation of the produced nanocomposite specimens [25]. U. Soy et al. studied the friction and wear behavior of the aluminum alloy AA360 reinforced with SiC, B_4C, and SiC/B_4C particles using the pressured infiltration method. Dry sliding wear behavior was carried out by a pin-on-disc machine under applied loads of 10, 20, and 30 N and sliding speeds of about 0.5, 1.0, and 1.5 ms^{-1}. The results of this investigation showed that the wear rates for Al/17 wt.% B_4C, Al/17 wt.% SiC/B_4C and Al/17 wt.% SiC are about 49, 79, and 160 percent, respectively. The friction coefficient of the manufactured composites is about 25–30 percent lower than the original aluminum alloy. The manufactured composites for the present work are important in many industrial applications owing to their lightweight and low wear rate. Microstructural analysis was defined by scanning electron microscopy and energy dispersion spectroscopy [26]. N. Altinkok et al. investigated the effect of Al_2O_3/SiC particles incorporated into an Al matrix manufactured via the stir-casting route. Hybrid ceramic powder Al_2O_3 + SiC was introduced at 10 wt.% and different particle sizes. The mixture of Al_2O_3 and SiC was introduced into the AA332 aluminum matrix and followed by heating at 1200 °C in inert gas. Dry sliding wear behavior was carried out using a pin-on-disc machine. The results of this study showed that the hybrid materials decreased wear rate, especially for coarse SiC particle sizes. This is attributed to the ability of coarse SiC to carry larger applied loads. Also, the hybrid mixture of ceramic Al_2O_3 and SiC will improve the hardness. The microstructural analysis was conducted using an optical microscope, which revealed a homogeneous distribution of Al_2O_3 and SiC in the AA332 matrix [27]. Serdar Salman et al. investigated the effect and characterization of ceramic coating on cast iron bases. In this work, three kinds of ceramic coating were used (Al_2O_3, ZrO_2, and Cr_2O_3), which are precipitated on cast iron by plasma spraying. Plasma spraying was conducted using a thermal shock test with a thermal torch according to an international standard. The result of this study showed that ZrO_2 coating has excellent properties compared with Al_2O_3 and Cr_2O_3, which enable it to be used for many engine parts [28]. M. Abbasi et al. studied the effect of each friction stir vibration processing (FSVP) as a new process to enhance the microstructure and mechanical properties of metal surface AA5052 and compared it with traditional friction stir processing (FSP). The metal surface of AA5052 was incorporated by SiC nanoparticles and then vibrated normally to the processing line through friction stir processing. Rotation and transverse motion of the shoulder are performed simultaneously with the vibration movement of the specimen. The results of this work show that the vibration motion during friction stir processing (FSP) leads to the refining grain size at the stirring zone and then creates a homogeneous distribution of nanoparticles at the surface of the AA5052 alloy. Also, the results reveal that the strength and ductility of FSVP are greater than those of FSP [29]. Moreover, many investigations have been published in friction stirring welding with SiC particles. M. Abbasi et al. added SiC to the Mg matrix. SiC particles were added during stirring to improve the strength and ductility of AZ31 magnesium alloy [30]. Mustafa Dadaei investigated the effect of SiC/Al_2O_3 during the friction-stirring processing of the AZ91 magnesium alloy. The results of this work show that SiC particles are more effective than Al_2O_3 in improving mechanical properties. This is owing to the good dispersion of SiC particles on the welding surface and the refining of the particles in the welding zone [31]. Amin Abdollahzadeh et al. studied the effect of SiC particles in the joining of aluminum and copper sheets during friction stir spot welding (FSSW). The results of this work show an improvement in mechanical properties such as strength to the good formation of $CuAl_2$, CuAl, Al_4Cu_9 and refining of the grains at the welding surfaces between Al and Cu sheets [32].

The aim of the present work is to produce Al/TiC and Al/B_4C using powder technology routes and make comparisons between them to define which one is preferred. The preferred nanocomposite was defined by studying the mechanical properties, physical properties and wear behavior. The difference between the present work and the previous study is that it uses two different types of carbide nanomaterials (TiC and B_4C).

2. Materials and Processing Methods

2.1. Raw Materials

Al powder type AA6061 was used at a particle size of 120 μm, while the reinforcing additives were B_4C and TiC at 40 nm in particle size. Tables 1 and 2 demonstrate the chemical composition of AA6061 powder [33]. Table 3 shows the physical and mechanical characteristics of B_4C and TiC [34].

Table 1. The components of aluminum alloy in wt.% [33].

Mg	Si	Fe	Cr	Cu	Zn	Ti	Mn	Al
0.81	0.59	0.21	0.19	0.19	0.08	0.08	0.018	Rem.

Table 2. Physical and mechanical characteristics of aluminum alloy [33].

Tensile Strength (MPa)	Micro-Hardness (HB-500)	Modulus of Elasticity (GPa)	Density (gm/cm^3)	Poisson's Ratio
115	30	70–80	2.7	0.33

Table 3. Physical and mechanical characteristics of B_4C and TiC [34].

Substance	Tensile Strength (MPa)	Micro-Hardness (MPa)	Poisson's Ratio	Modulus of Elasticity (GPa)	Melting Point (°C)	Density (g/m^3)
B_4C	261–569	3810	0.18–0.21	362–472	2350	2.5
TiC	258	3200	0.18–0.19	448–451	3160	4.93

2.2. Samples Preparing

The samples were produced using the powder metallurgy route, first mixing the raw materials with zinc stearate as an activator. The mixing process was conducted using a mixer (planetary ball mill QM-ISPO4) supplemented with steel balls for milling (1 cm in diameter) and rotating at 245 rpm for 3.5 h. After the mixing process, the powder mixture was pressed in uni-axial pressing at room temperature according to ASTM-D 618 [35] to obtain a green sample, and then the weight of the specimens was measured by a sensitive electronic balance to define the density of the green sample after the pressing process. After pressing, the specimens were sintered using an electrical furnace at 500 °C for 3.5 h, which was supplied by inert gas (argon) to inhibit the oxidation of the specimens. Afterwards, the density of sintered specimens was measured as well as the density of green samples.

2.3. Examination of the Microstructure

In the beginning, the specimens of AA6061/B_4C nanocomposites and AA6061/TiC were ground by grinding papers at particle sizes of 380 and 500 μm. Afterward, the samples were polished using a polishing apparatus with diamond paste at particle size 0.5 μm for 10 min, and then the specimens were etched with 1% Keller material for 0.5 min.

2.4. X-ray Diffraction Analysis

X-ray diffraction analysis was carried out for the nanocomposite samples (Al/TiC, Al/B_4C) to define the phases as a result of the powder metallurgy route. Furthermore, X-ray examination was used to study the effect of ceramic nanomaterials (TiC, B_4C) on the created phases of the prepared nanocomposites.

Theoretical and actual densities for (AA6061/TiC and AA6061/B_4C) were calculated by Archimedes principles depending on (ASTM C20-00) using the equations [36]:

$$\text{For (Al/TiC) } \rho_c = \frac{1}{\frac{w_{A1}}{\rho_{A1}} + \frac{w_{TiC}}{\rho_{TiC}}} \quad (1)$$

$$\text{For (Al/B}_4\text{C) } \rho_C = \frac{1}{\frac{w_{A1}}{\rho_{A1}} + \frac{w_{B4C}}{\rho_{B4C}}} \quad (2)$$

Equations (1) and (2) were used to measure theoretical density, while the actual density for all the sintered specimens was measured using the equation [36]:

$$\rho_s = \frac{m_a \times \rho_w}{m_a - m_w} \quad (3)$$

The percentage of porosity in the samples was measured using the following formula:

$$porosity\ \% = 1 - \frac{Ps}{P_{th}} \quad (4)$$

2.5. Micro-Hardness Testing

Micro-hardness testing was carried out using Rockwell micro-hardness device type (TESCAN MIRA3 FEG-SEM, Queensland, Australia), using scale type (B) with loading at 100 kg for the indenter. This testing was conducted for all the compacted and sintered specimens. At least four readings were taken to obtain the average diameter (d_{ave}) of the indenter for each specimen.

2.6. Wear Testing

Wear testing was conducted using a pin-on-disc machine for all the samples after sintering, depending on the ASTM-G99 standard. Wear testing was conducted on the samples at (2 cm in length and 1 cm in diameter). The wear testing was performed by applying loading at (3, 6, 9, 12 and 15 N) and a constant time of 10 min. The wear rate of the samples was measured by the weighing method. This method depends on measuring the losses in weight for all samples with a sensitive electronic balance of about (0.01 mg) accuracy. Figure 1 shows the schematic diagram of the wear-testing machine. Afterward, the wear rate was calculated using the formula [37]:

$$wear\ rate = \frac{\Delta w}{2\pi rnt} \quad (5)$$

$$\Delta w = w_1 - w_2 \quad (6)$$

$$S.D. = 2\pi \cdot r \cdot n \cdot t$$

where:

Δw: Change in weight (g).
w_1 and w_2: Weight of the specimen prior and after testing (gm).
r: Radius of the rotating disc (mm).
n: Number of the disc rotating's (rpm).
t: Testing time (min).

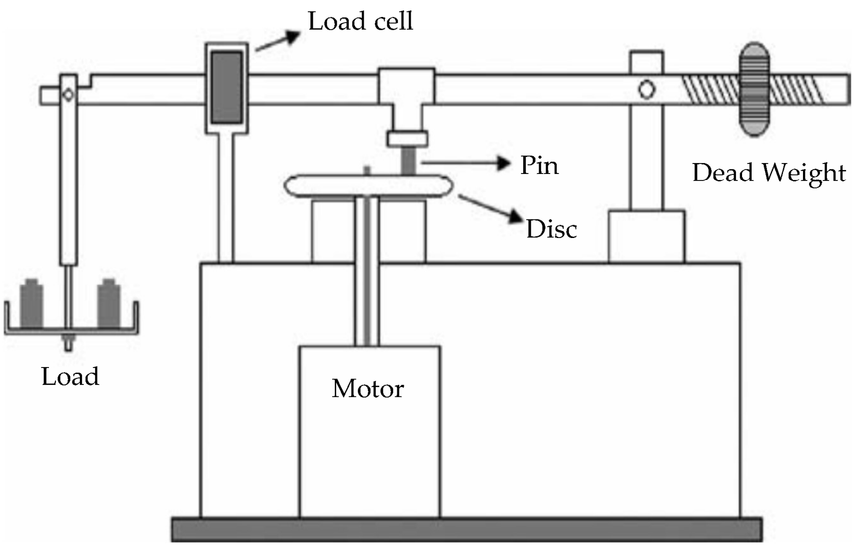

Figure 1. Schematic diagram of wear testing machine [26].

3. The Obtained Data and Their Discussion

3.1. Results of Microstructure Examination

Figure 2 shows the photomicrographs of the field emission scanning electron microscope (FESEM) for the AA6061 aluminum matrix and the fabricated nanocomposites Al/B_4C and Al/TiC with different percents of B_4C and TiC. The photomicrographs show that B_4C and TiC nanoparticles are diffused at the grain boundaries between the B_4C, TiC and Al matrix. Owing to the thermal reaction and diffusion mechanism created in the sintering process, strong bindings have been created at the grain boundaries between the ceramic nanoparticles B_4C, TiC and Al matrix. It can be revealed that B_4C and TiC nanoparticles may be wetted by aluminum matrix through the sintering process. Owing to the aggregation in a specific region, a homogeneity of B_4C and TiC in the Al matrix cannot be created in some specimens. Also, the difference in thermal properties between the Al matrix and B_4C and TiC nanoparticles plays a great role in the dispersion of B_4C and TiC nanoparticles into the Al matrix and then affects the wetting between the B_4C and TiC nanoparticles and the Al matrix.

3.2. Analysis of X-ray Diffraction Results

The phases of the manufactured samples were defined using the X-ray diffractometer 4lab model (XRD-6000) of SHIMADZU Europe with CuKα radiation and wavelength (1.54056 A°) for each sample. Figure 3a shows the X-ray diffraction peaks for (Al/B_4C) nanocomposites with different wt.% of B_4C (2.5 wt.%, 5 wt.%, 7.5 wt.%, 10 wt.% and 12.5 wt.%). Figure 3b shows the X-ray diffraction peaks for (Al/TiC) nanocomposites with different wt.% of TiC (2.5 wt.%, 5 wt.%, 7.5 wt.%, 10 wt.% and 12.5 wt.%).

As shown in Figure 3a XRD peaks for the samples (Al/B_4C) nanocomposites containing (2.5 wt.%, 5 wt.%, 7.5 wt.%, 10 wt.% and 12.5 wt.%) B_4C, the peaks occurring at 2θ ranging about 20.2031°, 22.5658°, 24.209°, 35.6016°, 37.9378°, 54.6941°, 64.2011° and 66.1823° with an hkl of about (101), (003), (012), (104), (021), (205), (125) and (220). Also, there are four peaks for Al occurred at 2θ ranging about 38.3011°, 45.2120°, 65.1901° and 79.0402° with an hkl of about (111), (200), (220) and (311), respectively. These peaks have emphasized that B_4C nanoparticles were distributed homogeneously in the Al matrix.

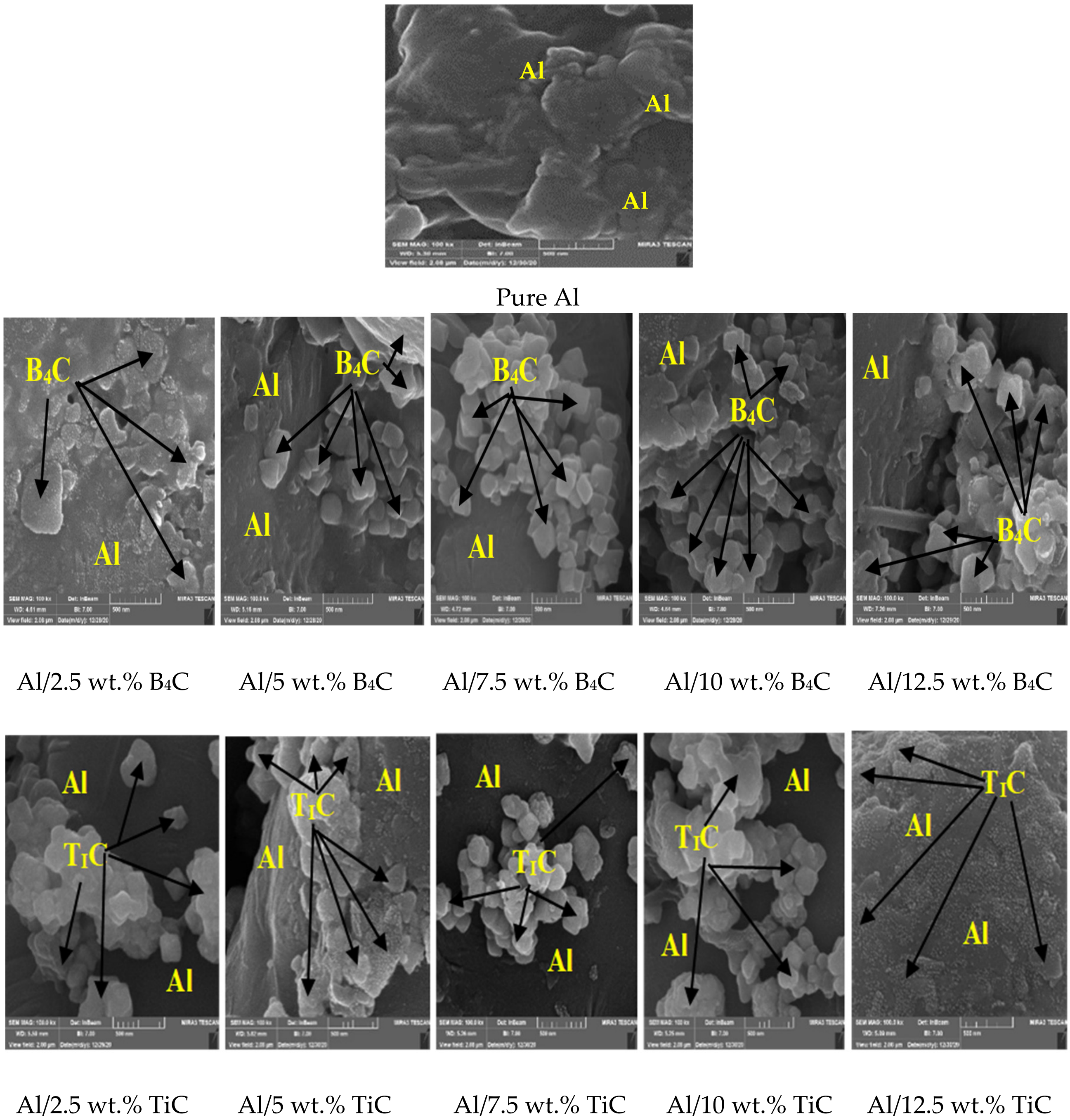

Figure 2. FESEM images of Al/B_4C and Al/TiC nanocomposites for different wt.%.

While Figure 3b shows XRD peaks for the samples (Al/TiC) nanocomposites containing (2.5 wt.%, 5 wt.%, 7.5 wt.%, 10 wt.% and 12.5 wt.%) TiC, the peaks occurred at 2θ ranging about 36.32°, 41.83°, 61.07° and 75.81° with an hkl of about (111), (200), (220) and (311). In addition, there are four peaks for Al appearing at 2θ ranging about 38.3011°, 45.2120°, 65.1901° and 79. 0402° with an hkl of about (111), (200), (220) and (311), respectively. These peaks indicate that TiC nanoparticles were distributed homogeneously in the Al matrix.

Each of the B_4C and TiC phases is strongly with Al particles due to the good wettability between them, improving their physical and mechanical properties.

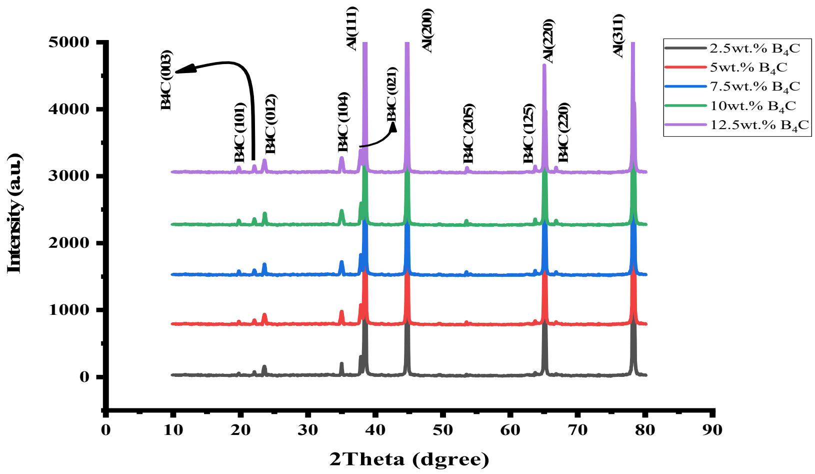

(**a**)

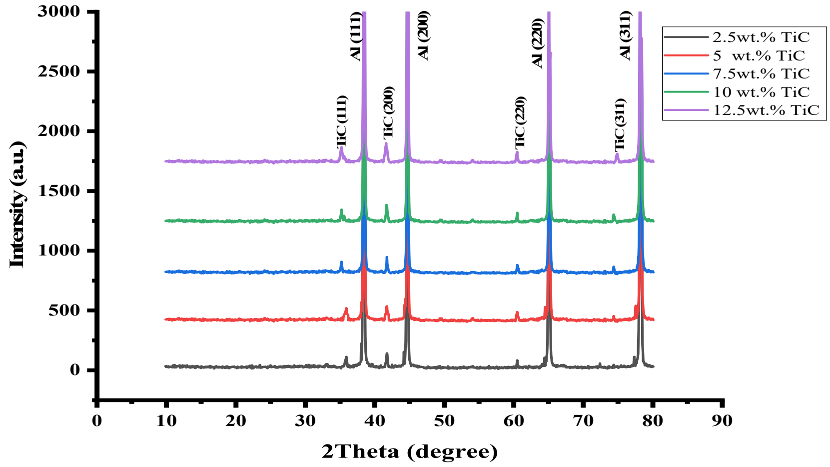

(**b**)

Figure 3. (**a**) XRD for Al/B_4C Nanocomposite. (**b**) XRD for Al/TiC Nanocomposite.

3.3. Mechanisms of Pressing and Sintering Processes

For the pressing process, the addition of B_4C nanoparticles increases the density after compacting because of the condensation process during the compacting process, as shown in Figure 4a. Afterward, all nanoparticles will close together owing to the increase in pressing force. For the sintering process, necking will be created between all nanoparticles of raw powders and the additive nanoparticles owing to the welding between them, which then causes shrinkage of the samples and increases the density of the sintered samples [38]. The temperature of the sintering process will create strong bindings at the interfaces between aluminum particles and the additive nanoparticles and then enhance the mechanical characteristics such as young modulus, ultimate strength, and micro-hardness. Therefore, binding forces have an extremely negative effect on the wear behavior of nanocomposites, and then increase the dislocations by interlocking and forming loops close to the reinforcing nanoparticles, which inhibit the movement of the dislocations [33]. The increment in the concentrations of B_4C reinforcing nanoparticles will increase the density of manufactured nanocomposites, as illustrated in Figure 4a. This leads to an increase in the wettability at the interfaces between the B_4C nanoparticles and Al particles. Moreover, much porosity can be formed at the interfacial regions of TiC nanoparticles and Al particles, decreasing the density of Al/TiC nanocomposites, as shown in Figure 4b. On the other hand, the porosity decreases with increasing B_4C and increases with increasing TiC, and then the porosity of Al/B_4C nanocomposites is lower than for Al/TiC, as demonstrated in Figure 5.

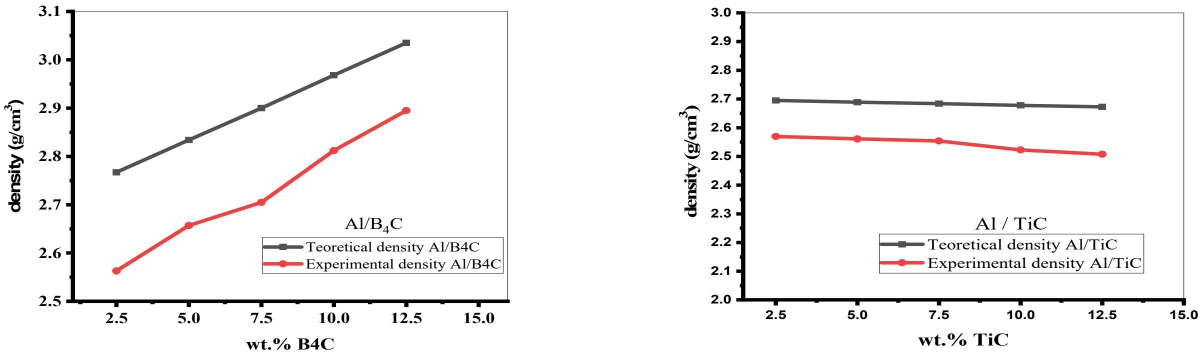

(**a**) (**b**)

Figure 4. (**a**) Show the experimental and (**b**) Show the experimental and theoretical densities vs. wt.% of B_4C and theoretical densities vs. wt.% of TiC.

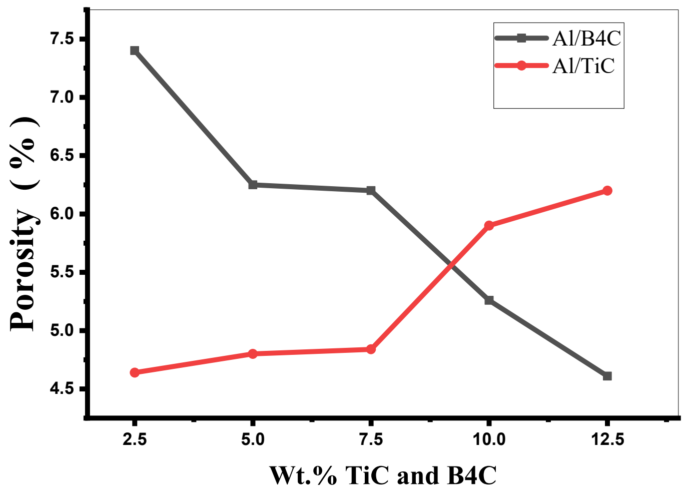

Figure 5. Show the porosity (%) vs. wt.% of B_4C and TiC.

3.4. Wear Testing

The wear rate for Al/B_4C and Al/TiC nanocomposites is extremely dependent on the reinforcing nanoparticles and their concentrations. The increase in wt.% of B_4C and TiC leads to decreased wear rate (increasing wear resistance), this is due to the bindings at the interfaces between the reinforcing nanoparticles and Al particles, and then creating thermal stresses at their interfaces because of the differences in melting points of the reinforcing nanoparticles and aluminum particles, and then these thermal stresses will increase the dislocations interlocking.

The reinforcing nanoparticles will inhibit the movement of dislocations and increase wear resistance (decreasing wear rate). Figure 6 shows that the increment of B_4C will decrease the wear rate more than TiC, which is in line with [33]. The increment in applied loading at a constant time will increase the wear rate of Al/B_4C and TiC. Increasing the friction between the sample (Al/B_4C, Al/TiC) and the disc will increase the temperature and then create thin oxidized films. Afterwards, thin oxidation film will be fragmented and grooved at worn surfaces; this is in agreement with [39]. Figure 6 depicts the relationships between wear rate and applied loading for different wt.% of nanoparticles. The increment in applied loading will increase the wear rate for all samples. The wear rate of nanocomposites reinforcing by B_4C is lower than for TiC and pure Al particles as a matrix for many reasons mentioned previously.

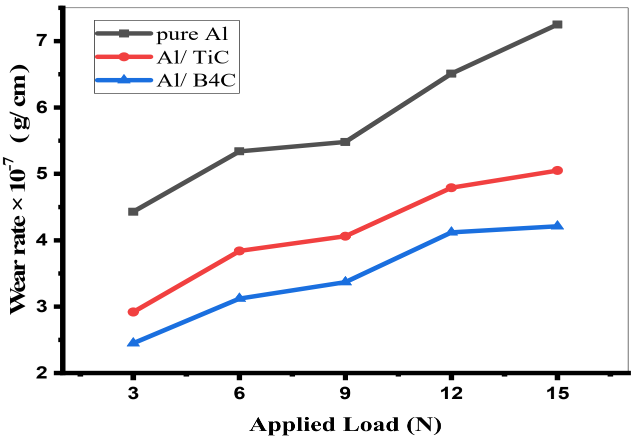

Figure 6. Show wear rate vs. applied loading.

The surface topography of nanocomposites was analyzed by an ordinary optic microscope (OM), as shown in Figure 7, which depicts the grooves of the surfaces for Al/B_4C and Al/TiC nanocomposites. The grooves of Al/B_4C nanocomposites are finer than the grooves of Al/TiC nanocomposites because the B_4C nanoparticles are harder than the TiC nanoparticles. Adhesive and abrasive wear are created for all the specimens. At lower loads, abrasive wear is the main wear mechanism, while at higher loads, adhesive wear is the major wear mechanism. For Al/B_4C nanocomposites and Al/TiC nanocomposites, there are adhesive wear and abrasive wear will be created. This agrees with [27].

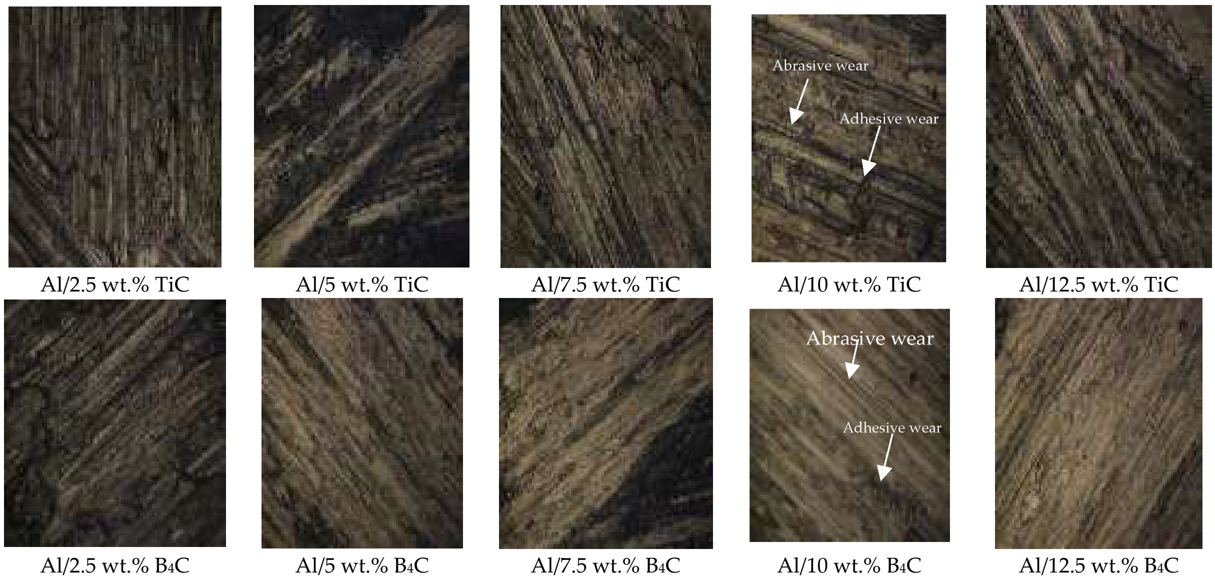

Figure 7. Photomicrographs of the grooves for Al/TiC and Al/B_4C nanocomposites at (6 N).

3.5. Micro-Hardness Characteristics

The microhardness of the synthesized nanocomposites extensively depends on the particle size of theadditive nanoparticles and their concentrations. The increment in the weight percentages of B_4C will increase the dislocation interlocking more than for TiC and then improve the microhardness. The microhardness of Al/B_4C nanoparticles is higher than that of Al/TiC nanoparticles; hence, the B_4C reinforcing nanoparticles create stronger bonds with Al particles than the TiC reinforcing nanoparticles, which then inhibit the movement of the dislocations and in turn increase the microhardness, as shown in Figure 8. Moreover, the microhardness values of Al/B_4C and Al/TiC nanocomposites are normally affected by compacting pressure, sintering temperature, and the weight percent of B_4C and TiC. The microhardness increases with increasing weight percents of B_4C and TiC.

This is due to the higher hardness of each B_4C and TiC matrix than the Al matrix. Finally, the micro-hardness test is a valuable route to define the microstructure and mechanical properties of nanocomposites. As shown in Figure 8, the values of micro-hardness for Al/B_4C nanocomposites and Al/TiC are 92 (HRC) and 87.4 (HRC), respectively.

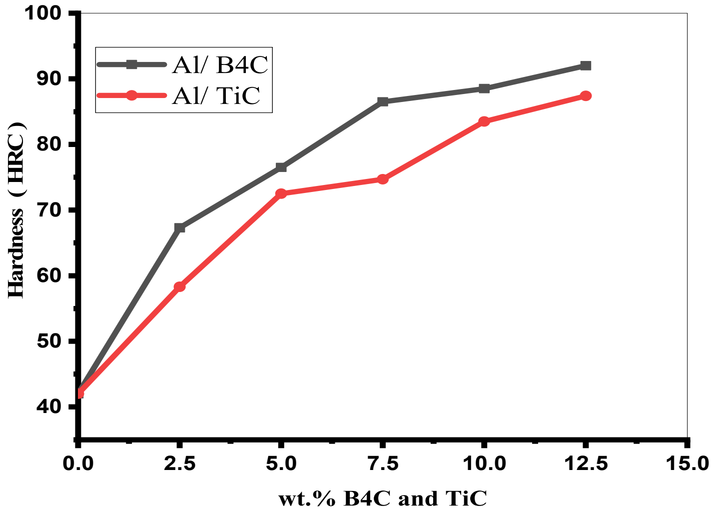

Figure 8. Show relationships between microhardness and wt.% of B_4C and TiC.

4. Conclusions

The effect of B_4C and TiC nanoparticles on the microstructure and mechanical properties of the AA6061 aluminum alloy was investigated in the present work. Al/B_4C and Al/TiC were manufactured using a powder metallurgy route. The images of field emission scanning electron microscopy (FESEM) showed a homogeneous dispersion of B_4C and TiC into the AA6061 matrix. The results showed that Al/B_4C specimens 92 (HRC) had higher micro-hardness with respect to Al/TiC specimens 87.4 (HRC). For the same concentration of B_4C and TiC nanoparticles, the effect of B_4C nanoparticles on the enhancement of microstructure and mechanical properties was higher than that for TiC ones. Additionally, it was indicated that the wear rate of Al/B_4C and Al/TiC increased as the applied load increased. It was shown that the wear rates of Al/B_4C and Al/TiC were 4.21×10^{-7} (g/cm) and 5.1×10^{-7} (g/cm), respectively. The increment of B_4C nanoparticles percents increased the actual density, while the increment of TiC nanoparticles percents slightly decreased the actual density. Also, the increment of B_4C nanoparticles percent decreased the porosity by (4.61%), while the increment of TiC nanoparticles percent increased the porosity by (6.2%). Finally, the powder metallurgy route to produce Al/B_4C and Al/TiC nanocomposites is recommended to enhance the microstructure and wear properties of the AA6061 alloy.

Author Contributions: Methodology, L.K.H. and S.M.J.; investigation, L.K.H., S.M.J., K.D.S. and W.A.K.A.-M.; writing—original draft preparation, L.K.H., S.M.J., K.D.S. and W.A.K.A.-M.; writing—review and editing, L.K.H., S.M.J., K.D.S. and W.A.K.A.-M.; supervision, F.A. and B.E. All authors have read and agreed to the published version of the manuscript.

Funding: All authors certify that they have no affiliations or involvement with any organization or entity with any financial or non-financial interest in the subject or material discussed in this manuscript. This research received no external funding.

Data Availability Statement: The data presented in this study are available on request from the corresponding author. The data are not publicly available due to privacy.

Acknowledgments: We acknowledge support by the Deutsche Forschungsgemeinschaft (DFG—German Research Foundation) and the Open Access Publishing Fund of the Technical University of Darmstadt. The authors would like to also thank the University of Technology-Iraq.

Conflicts of Interest: The authors declare no conflict of interest.

References

1. Khazaal, S.M.; Namer, N.S.M.; Szabolcs, S.; Al Ansari, L.S.; Sammad, H.J.A. Study of manufacturing and material properties of the hybrid composites with metal matrix as tool materials. *J. Results Eng.* **2022**, *16*, 100647. [CrossRef]
2. Behera, M.P.; Dougherty, T.; Singamneni, S. Conventional and additive Manufacturing with Metal Matrix Composites: A Perspectivc. *Procedia Manuf.* **2019**, *30*, 159–166. [CrossRef]
3. Jawalkar, C.; Verma, A.S.; Suri, N. Fabrication of aluminum metal matrix composites with particulate reinforcement: A review. *Mater. Today Proc.* **2017**, *4*, 2927–2936.
4. Salman, K.D.; Al-Maliki, W.A.K.; Alobaid, F.; Epple, B. Microstructural Analysis and Mechanical Properties of a Hybrid Al/Fe2O3/Ag Nano-Composite. *Appl. Sci.* **2022**, *12*, 4730. [CrossRef]
5. Acikgoz, A.; Aktas, B.; Demircan, G.; Amasyah, F.; Akdemir, F. Characterization of Nano Aluminum Oxide Reinforced Iron Composites Produced by Powder Metallurgy. In Proceedings of the Fourth International Iron & Steel Symposium, Karabük, Turkey, 4–6 April 2019; pp. 351–355.
6. Salman, K.D.; Al-Maliki, W.A.K.; Alobaid, F.; Epple, B. Microstructural Analysis and Mechanical Characterization of Shape Memory Alloy Ni-Ti-Ag Synthesized by Casting Route. *Appl. Sci.* **2022**, *12*, 4639. [CrossRef]
7. Ponnusamy, P.; Rashid, R.A.; Masood, S.H.; Ruan, D.; Palanisamy, S. Mechanical Properties of imprinted aluminum alloys: A review. *Materials* **2020**, *13*, 4301. [CrossRef]
8. Awotuncle, M.A.; Adegbenjo, A.O.; Obaded, B.A.; Okovo, M.; Shongwe, B.M.; Olubambi, P.A. Influence of sintering methods on the mechanical properties of aluminum nanocomposites reinforced with carbonaceous compounds: A review. *J. Mater. Res. Technol.* **2019**, *8*, 2432–2449. [CrossRef]
9. Aatthisugan, I.; Muralidharan, S.; Majumdar, S.; Rose, A.R.; Jebadurai, D.S. Wear and mechanical properties of Al-6% Cu-X% Mg alloy fabricated by powder metallurgy. *IOP Conf. Ser. Mater. Sci. Eng.* **2018**, *402*, 012106. [CrossRef]
10. Manikanden, R.; Arjunan, T. Studies on microstructural characteristics, mechanical and tribological behaviors of boron carbide and cow dung ash reinforced aluminum (Al 7075) hybrid metal matrix composite. *Compos. Part B Eng.* **2020**, *183*, 107668. [CrossRef]
11. Chintada, S.; Dora, S.P.; Kare, D.; Pujari, S.R. Powder metallurgy versus casting: Damping behavior of pure aluminum. *J. Mater. Eng. Perform* **2022**, *31*, 9122–9128. [CrossRef]
12. Kumar, D.; Angra, S.; Singh, S. Mechanical Properties and Wear Behavior of Stir Cast Aluminum Metal Matrix Composite: A Review. *Int. J. Eng. Trans. A Basics* **2022**, *35*, 794–801.
13. Salman, K.D. Synthesis and Characterization Unsaturated Polyester Resin Nanocomposites Reinforced by Fe_2O_3+ Ni Nanoparticles: Influence on Mechanical and Magnetic Properties. *Int. J. Eng. Trans. A Basics* **2022**, *35*, 21–28.
14. Aswad, M.A.; Awad, S.H.; Kayyem, A.H. Study on Iraqi Bauxite Ceramic Reinforced Aluminum Metal Matrix Composite Synthesized by Stir Casting. *Int. J. Eng. Trans. A Basics* **2020**, *33*, 1331–1339.
15. Selvan, J.D.R.; Dinaharan, I.; Mashinini, P.M. High temperature sliding wear behavior of AA6061/fly ash aluminum matrix composites prepared using compo casting process. *Tribol. Mater. Surf. Interfaces* **2017**, *11*, 39–46.
16. Golestanipour, M.; Aysak, H.K.; Sasani, N.; Sadeghian, M.H. A Novel, Simple and Cost-Effective Al A356/ Al_2O_3 Nano-composite Manufacturing Rout with Uniform Distribution of Nanocomparticles. *Int. J. Eng. Trans. A Basics* **2015**, *28*, 1320–1327.
17. Kaushik, N.; Singhal, S. Experimental Investigations on Microstructural and Mechanical Behavior of Friction Stir Welded Aluminum Matrix Composite. *Int. J. Eng. Trans. A Basics* **2019**, *32*, 162–170.
18. Wu, Y.; Zhan, K.; Yang, Z.; Sun, W.; Zhao, B.; Yan, Y.; Yang, J. Graphene oxide/Al composites with enhanced mechanical properties fabricated by simple electrostatic interaction and powder metallurgy. *J. Alloys Compd.* **2019**, *775*, 233–240. [CrossRef]
19. Tian, W.; Qin, G.Q.; Liang, Q.C. Effects of sintering temperature on microstructure and wear properties of Al_2O_3 particle reinforced Al composites. *Adv. Mater. Res.* **2015**, *1095*, 16–19.
20. Venkatesh, B.; Harish, B. Mechanical Properties of Metal Matrix Composites (Al SiCp) Particles Produced by Powder Metallurgy. *Int. J. Eng. Res. Gen. Sci.* **2015**, *3*, 1277–1284.
21. Thangarasu, A.; Murugan, N.; Dinaharan, I.; Vijay, S.J. Synthesis and Characterization of titanium carbide particulate reinforced AA 6082 aluminum alloy composites via friction stir processing. *Arch Civ. Mech. Eng.* **2015**, *15*, 324–334. [CrossRef]
22. Manohar, G.; Maity, S.R.; Pandey, K.M. Microstructural and mechanical properties of microwave sintered AA7075/ graphite/ SiC hybrid composite fabricated by powder metallurgy techniques. *Silicon* **2022**, *14*, 5179–5189. [CrossRef]
23. Negin, A.; Hanim, A.; Sarraf, M.; Sulaiman, S.; Hong, T.S. Microstructural, Tribology and Corrosion Properties of Optimized Fe_3O_4-SiC Reinforced Aluminum Matrix Hybrid Nano Filler Composite Fabricated through Powder Metallurgy Method. *Materials* **2020**, *13*, 4090.
24. Li, G.; Xiong, B. Effects of graphene content on microstructures and tensile property of graphene-nanosheets/ aluminum composites. *J. Alloys Compd.* **2017**, *697*, 31–36. [CrossRef]
25. Maleki, A.; Taherizadeh, A.R.; Issa, H.K.; Niroumand, B.; Allafchian, A.R.; Ghaei, A. Development of a new magnetic aluminum matrix nanocomposite. *Ceram. Int.* **2018**, *44*, 15079–15085. [CrossRef]
26. Soy, U.; Demir, A.; Findik, F. Friction and wear behaviors of Al-SiC-B_4C composites produced by pressure infiltration method. *Ind. Lubr. Tribol.* **2011**, *63*, 387–393. [CrossRef]
27. Altınkok, N.; Özsert, I.; Fındık, F. Dry Sliding Wear Behavior of Al_2O_3/SiC Particle Reinforced Aluminium Based MMCs Fabricated by Stir Casting Method. *Acta Phys. Pol. A* **2013**, *124*, 11–19. [CrossRef]

28. Salman, S.; Köse, R.; Urtekin, L.; Findik, F. An investigation of different ceramic coating thermal properties. *J. Mater. Des.* **2006**, *27*, 585–590. [CrossRef]
29. Abbasi, M.; Givi, M.; Ramazani, A. Friction stir vibration processing: A new method to improve the microstructure and mechanical properties of Al5052/SiC surface nanocomposite layer. *Int. J. Adv. Manuf. Technol.* **2019**, *100*, 1463–1473. [CrossRef]
30. Abbasi, M.; Abdollahzadeh, A.; Bagheri, B.; Omidvar, H. The effect of SiC particle addition during FSW on microstructure and mechanical properties of AZ31 magnesium alloy. *J. Mater. Eng. Perform.* **2015**, *24*, 5037–5045. [CrossRef]
31. Dadaei, M.; Omidvar, H.; Bagheri, B.; Jahazi, M.; Abbasi, M. The effect of SiC/Al2O3 particles used during FSP on mechanical properties of AZ91 magnesium alloy. *Int. J. Mater. Res.* **2014**, *105*, 369–374. [CrossRef]
32. Amin, A.; Bagheri, B.; Shamsipur, A. Development of Al/Cu/SiC bimetallic nano-composite by friction stir spot welding. *Mater. Manuf. Process.* **2023**, *38*, 1416–1425.
33. Balaji, P.; Arun, R.; JegathPriyan, D.; Ram, I.M.; Manikandan, E. Comparative study of Al 6061 alloy with Al 6061-magnesium oxide (MgO) composite. *Int. J. Sci. Eng. Res.* **2015**, *6*, 408.
34. AZOM. AZO Materials. Available online: https://www.azom.com/ (accessed on 2 May 2023).
35. *ASTM-D 618*; Standard Practice for Conditioning Plastics for Testing. ASTM International: West Conshehoken, PA, USA, 2021.
36. Zaid, H.M.; Abed, A.R.; Hasan, H.S. Improvement of Mechanical properties of Magnesium (Mg) Matrix Composites Reinforced with Nano Alumina (Al_2O_3) Particles. In Proceedings of the IOP Conference Series: Material Science and Engineering, Chennai, India, 16–17 September 2020; IOP Publishing: Bristol, UK; Volume 67, p. 012162.
37. Bayraktar, E.; Katundi, D.; Ferreira, L.M.; Robert, M.H. Design and microstructural evolution, mechanical and physical properties of fine particles reinforced aluminum matrix composites. *Adv. Mater. Process. Technol.* **2016**, *2*, 566–577.
38. Krishna, S.M.; Shridhar, T.N.; Krishnamurthy, I. Evaluation and examination of volume fraction, porosity, microstructure and computational modeling of hybrid metal matrix composites to reveal the heat flow distribution characteristics. *Int. J. Mater. Sci. Eng.* **2015**, *3*, 231–243.
39. Alaneme, K.K.; Fajemisin, A.V.; Maledi, N.B. Development of aluminum-based composites reinforced with steel and graphite particles: Structural, mechanical and wear characterization. *J. Mater. Res. Technol.* **2019**, *8*, 670–682. [CrossRef]